Large amplitude whistlers in the magnetosphere observed with Wind-Waves

P. J. Kellogg,[1] C. A. Cattell,[1] K. Goetz,[1] S. J. Monson,[1] and L. B. Wilson III[2]

Received 10 July 2010; revised 9 June 2011; accepted 27 June 2011; published 21 September 2011.

[1] We describe the results of a statistical survey of Wind-Waves data motivated by the recent STEREO/Waves discovery of large-amplitude whistlers in the inner magnetosphere. Although Wind was primarily intended to monitor the solar wind, the spacecraft spent 47 h inside 5 R_E and 431 h inside 10 R_E during the 8 years (1994–2002) that it orbited the Earth. Five episodes were found when whistlers had amplitudes comparable to those of Cattell et al. (2008), i.e., electric fields of 100 mV/m or greater. The whistlers usually occurred near the plasmapause. The observations are generally consistent with the whistlers observed by STEREO. In contrast with STEREO, Wind-Waves had a search coil, so magnetic measurements are available, enabling determination of the wave vector without a model. Eleven whistler events with useable magnetic measurements were found. The wave vectors of these are distributed around the magnetic field direction with angles from 4 to 48°. Approximations to observed electron distribution functions show a Kennel-Petschek instability which, however, does not seem to produce the observed whistlers. One Wind episode was sampled at 120,000 samples s^{-1}, and these events showed a signature that is interpreted as trapping of electrons in the electrostatic potential of an oblique whistler. Similar waveforms are found in the STEREO data. In addition to the whistler waves, large amplitude, short duration solitary waves (up to 100 mV/m), presumed to be electron holes, occur in these passes, primarily on plasma sheet field lines mapping to the auroral zone.

Citation: Kellogg, P. J., C. A. Cattell, K. Goetz, S. J. Monson, and L. B. Wilson III (2011), Large amplitude whistlers in the magnetosphere observed with Wind-Waves, *J. Geophys. Res.*, *116*, A09224, doi:10.1029/2010JA015919.

1. Introduction

[2] The importance of whistler mode waves to understanding the variability of the trapped energetic particles in the Earth's radiation belts has long been recognized [*Kennel and Petschek*, 1966; *Roth et al.*, 1999; *Horne et al.*, 2005; *Millan and Thorne*, 2007, and references therein]. Stimulated by the discovery of large amplitude whistlers with STEREO/Waves [*Cattell et al.*, 2008] we have searched for similar events in the data from Wind-Waves, which carries similar instrumentation [*Bougeret et al.*, 1995, 2008], but which also carries a search coil for magnetic fields in the whistler frequency range. Although Wind was primarily intended to monitor the solar wind, the spacecraft spent 47 h inside 5 R_E and 431 h inside 10 R_E during the 8 years that it orbited the Earth. A computer search of the entire part of the mission in Earth orbit found five episodes in which whistlers had large electric field amplitudes, defined as exceeding 100 mV/m and several more with amplitudes within an order of magnitude of those found by *Cattell et al.* [2008].

[3] Most of the waveforms of intense whistlers show a characteristic distortion, which we interpret as trapping of electrons. A full demonstration that this interpretation is correct involves use of both STEREO/Waves [*Bougeret et al.*, 2008], and Wind-Waves data and is published in another paper [*Kellogg et al.*, 2010].

[4] It is generally believed that whistlers may play an important role in the energization and loss of electrons in the magnetosphere [e.g., *Roth et al.*, 1999; *Omura et al.*, 2007; *Millan and Thorne*, 2007; *Cattell et al.*, 2008; *Bortnik et al.*, 2008], but the details are still uncertain. A better understanding of whistler wave properties is critical to an understanding of energetic particle acceleration and loss in the radiation belts of the Earth. Such understanding is already being developed as the *Cattell et al.* [2008] observations and similar observations from THEMIS [*Cully et al.*, 2008] are used in modeling [e.g., *Bortnik et al.*, 2008].

[5] The search also found, at greater radial distances on plasma sheet field lines mapping to the auroral zone, episodes of intense solitary waves with properties consistent

[1]School of Physics and Astronomy, University of Minnesota, Minneapolis, Minnesota, USA.
[2]NASA, Goddard Space Flight Center, Greenbelt, Maryland, USA.

Copyright 2011 by the American Geophysical Union.
0148-0227/11/2010JA015919

Table 1. Characteristics of the Five Episodes of Large Amplitude Whistlers

Period	AE	TDSS	f_p kHz	f_{ce} kHz	Ratio
11/13/1998, 18:10–18:22	NA	3E	145	12.9	0.089
04/10/2000, 02:45–03:15	604,609	3E	90	4.7	0.055
05/25/2000, 22:30–24:00	468,742	3B	85	3.8	0.045
08/15/2000, 18:00–19:00	118,146	3B	140	11.0	0.079
10/10/2002, 02:30–02:45	393,405	3B	28	14.0	0.5
10/10/2002, 02:59	same	3B	5	8.1	1.6

with electron holes similar to those studied by *Ergun et al.* [1998a, 1998b] and others.

2. Search Method

[6] A full description of the Wind-Waves experiment is in *Bougeret et al.* [1995]. In this paper we use measurements from the Time Domain Sampler (TDS) subsystem which makes rapid digitized samples of waveforms from the electric antennas and magnetic search coils. Waveforms are sampled at two rates, called TDSF (fast) and TDSS (slow). On-board algorithms select sets of samples, called "events," for telemetry to ground. The sampling rates may be as high as 120,000 samples per second, with event lengths of 2048 samples, and so only a tiny fraction of the data thus obtained can be telemetered. For TDSF, the on-board selection algorithm simply chooses the event with the largest amplitude. The triggering of TDSS was sometimes keyed to the fast trigger, but generally TDSS was given less telemetry.

[7] There were 3 electric dipoles, X, Y, and Z. X was composed of two wire monopoles 50 m long, Y was two wire monopoles 15 m long, and Z was a pair of 6 m long tube monopoles. The TDSF was always connected to two of the electric antennas, the connection being chosen by command. There was also a three axis search coil for magnetic measurements. The TDSS was connected to four of the six possible antennas, with an additional possibility of using a DC coupled preamplifier which responded down to zero frequency on the electric antennas. In operation, the DC preamp was most commonly used by the TDSS for the electric antennas, but the connections alternated between 3 electric antennas and one component of the search coil, and the opposite, 3 components of the search coils and one electric antenna.

[8] Some difficulty was experienced in finding a computer algorithm which reliably picked out whistlers from the 8 year data set without too many false positives. The early searches sought whistlers in the magnetic field data from TDSS, and these produced far too many false positives due to various "glitches," from magnetic interference. In the end, it was decided to look for events whose presentation was similar to those of STEREO, that is, to use the TDSF measurements of electric field. The following criteria picked out a set with about 90% false positives, but which was small enough for visual inspection of the plotted waveforms in the course of a few days. The algorithm required that (1) Wind be within 15 Earth radii, (2) a hodogram of the X and Y electric fields had an eccentricity larger than $(0.2)^2$ (ratio of the largest eigenvalue of the variance matrix to the smallest, note that eigenvalues are amplitudes squared) and (3) amplitudes on both X and Y antennas greater than 10 mV/m.

[9] It was then found that a large number of the false positives were electron holes, and these will also be discussed in section 6. The fact that the electric field of an electron hole is often unipolar in one direction and bipolar in an orthogonal direction imitates the eccentricity of a whistler, and the amplitudes of those we found were quite large.

[10] When a true whistler episode was identified, visual inspection of the waveforms for a few hours around the identified whistlers usually turned up a few more. A majority of the misses were due to a failure to telemeter the measurements in the X and Y directions in successive packets, required for the eccentricity calculation, and were not due to significant failure of the search criteria.

[11] These criteria identified five episodes with large amplitude whistlers. Although five episodes seems like a small number of events for a spacecraft which spent 8 years in orbit around the Earth, it is a significant fraction of the 17 perigees which were within 5 R_E, so that such large whistlers are not rare. In a statistical survey of 13 Wind perigee passes performed by eye, 12 were found to have large amplitude whistlers [*Wilson et al.*, 2011]. Note that, in addition to the *Cattell et al.* [2008] STEREO observation of large amplitude whistlers, THEMIS [*Cully et al.*, 2008] has observed whistlers with amplitudes of 100s of mV/m. Cluster [*Santolík et al.*, 2003] observed waves with amplitudes of 10 s of mV/m. After the conditions for the occurrence of whistlers were better understood, several episodes of whistlers in the 10 mV/m range were found. Although they are quite common they will not be further discussed in this paper.

[12] Table 1 summarizes some of the characteristics of the five episodes. The first column gives the times of the episodes of strong whistlers, the second gives the AE index for the hour before and the hour during the observations. The third shows the configuration of the TDSS (3E indicates a mode with 3 electric antennas and one search coil, 3B indicates 3 search coil components and one electric component). The last columns give the plasma frequency, the electron cyclotron frequency and their ratio.

[13] In most cases, the plasma frequency was determined from densities given at the NSSDC from the 3DP experiment, but in a few cases it was possible to see the plasma and upper hybrid lines in the radio spectrum so these were then used. Note that several of the episodes are concurrent with large AE index, indicating a substorm in progress or just finished.

[14] As described above, the successful search method used the measurements of electric fields, and these from the higher frequency channel of the TDS (TDSF). Each of the large whistler episodes was then examined for TDSS events. Of the five episodes of strong whistlers, TDSS waveforms with 3 components of the search coils were only available for three. In all, 13 TDSS events with 3 component search coil data were found. Of these, 11 were suitable for analysis. The advantage of 3 component magnetic field measurements is, of course, that the direction of the wave vector, **k,** can be determined directly from the measurements by finding the minimum variance direction, rather than by inference from the dispersion relation, observed density, and the consequent theoretical values for the fields. These

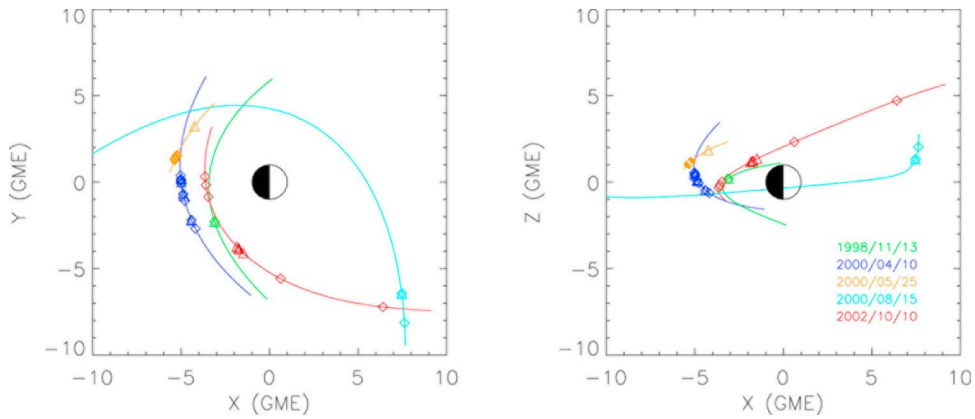

Figure 1. Locations where large amplitude whistlers were found. Triangles mark the TDSS events, and diamonds mark the TDSF events.

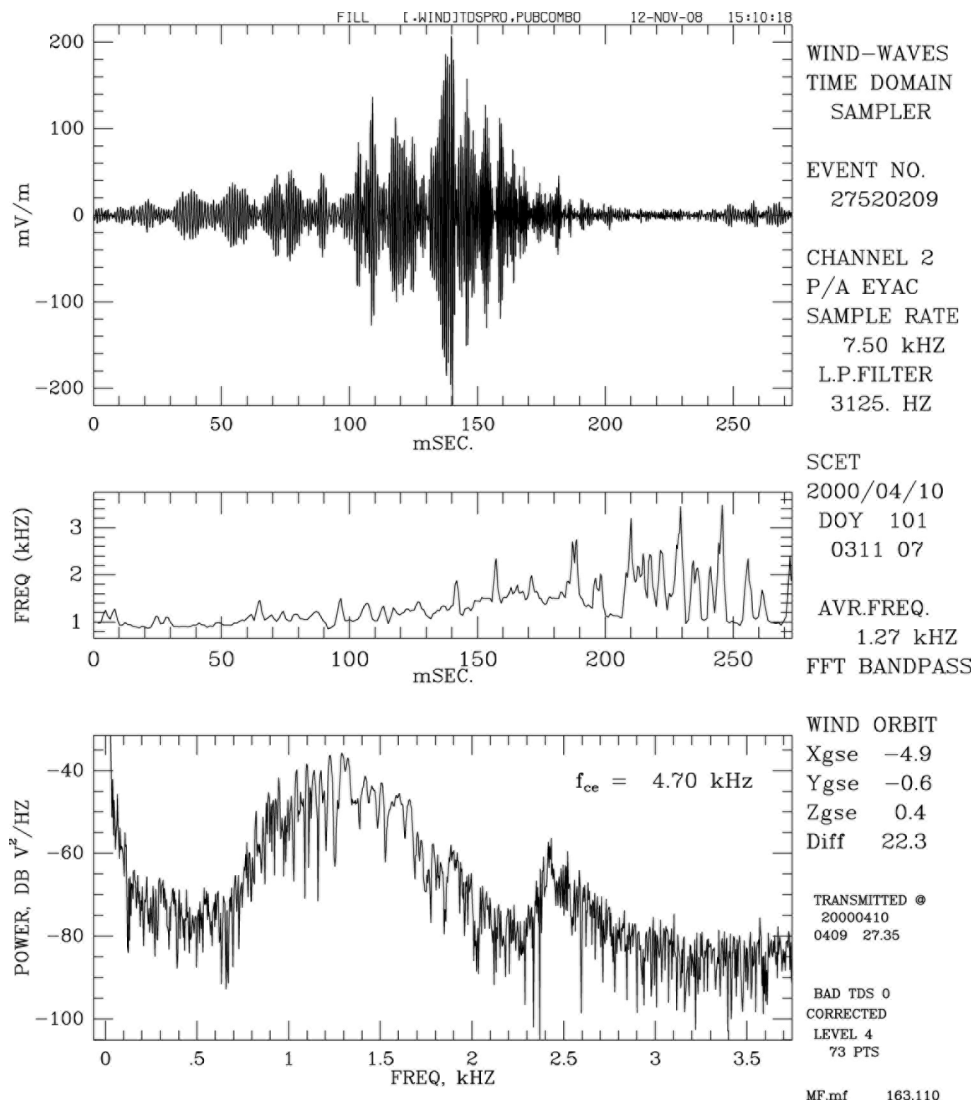

Figure 2. A typical large whistler burst. The frequency is obtained from zero crossings and is seen to increase appreciably during the burst.

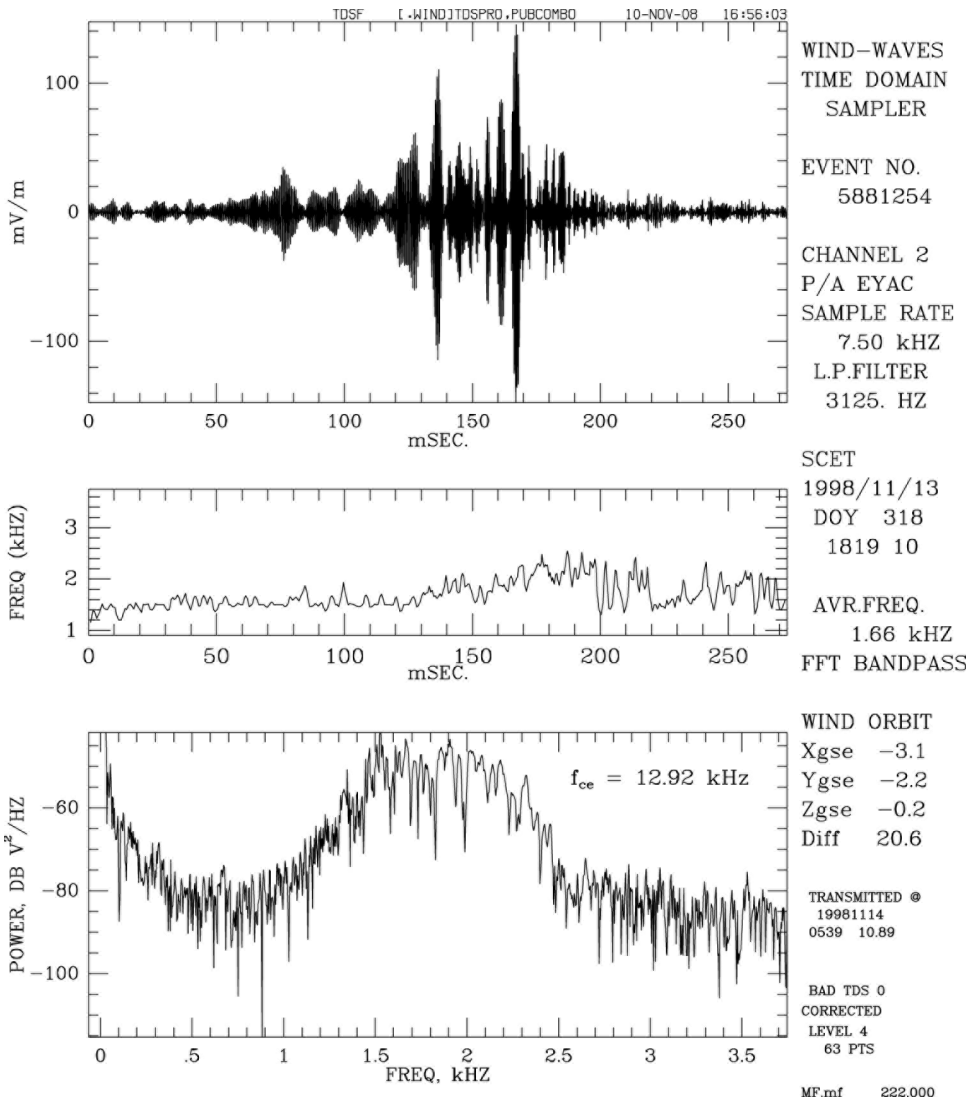

Figure 3. A whistler event showing that the increase of frequency is not due to the usual whistler dispersion.

measurements showed that the determination of obliquity from the eccentricity of the electric field hodogram in the plane perpendicular to B is not always accurate, though it is a reliable indicator that the whistler is strongly oblique.

3. Observations

[15] Figure 1 shows the regions where large amplitude whistlers were observed. Diamonds indicate TDSF events and triangles indicate TDSS events. Most of the whistlers were observed in a region similar to those of STEREO, namely at about 5 R_E on the post midnight sector of the nightside, and near the edge of the plasmasphere as determined from the plasma frequency as well as the location. However, whistlers were also observed at some surprising places, as the late events of 2002/10/10 which were sunward of the Earth and at higher latitude. The late events of this series were somewhat smaller than the rest, reaching only 30 mV/m and had higher frequency compared to the electron cyclotron frequency.

[16] Figure 2 displays, in the top panel, one component of the electric field waveform of one of the largest whistlers observed by TDSF. These observations are similar to those made on STEREO [*Cattell et al.*, 2008], that is, they are observations of the electric field. As with the STEREO whistlers, the signals are extremely bursty, and the most intense part of the signal lasts only a few msec. The second panel shows the frequency obtained from the intervals between zero crossings, showing that the frequency increases during the strongest part of a burst. The lowest panel shows the power spectrum for the entire event.

[17] Many, but not all, of the events show this increase which does not seem to be due to the dispersion of whistler signals. For whistlers below 1/4 of the cyclotron frequency, the higher frequencies have a higher group velocity and should arrive first. More accurately, the criterion should be 1/4 of the cyclotron frequency multiplied by cos θ. For the event shown in Figure 2, the frequency may be greater than 1/4 f_{ce} cos θ. The observations of Figure 2 were made when Wind was at a magnetic latitude of 1.3°N, very close to the

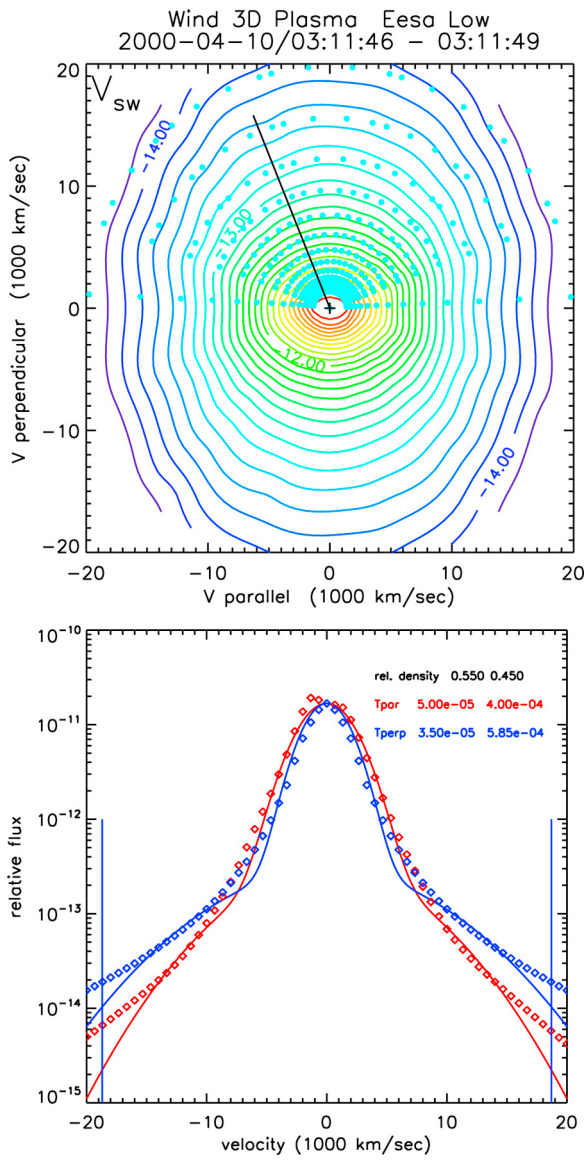

Figure 4. (top) Electron distribution during the event of Figure 2, from the 3DP experiment. (bottom) Cuts through the distribution together with calculated functions from a two bi-Maxwellian approximation. Temperatures are given in units of mc^2.

region where whistlers are often thought to be generated, so there perhaps has been little distance for dispersion Figure 3 shows a similar event, but one which argues again against dispersion as the explanation for the frequency increase. The frequency is about 1.6 kHz when it starts to increase. The angle k to B is not measured in this event, but no event has been found for which the angle exceeded 48°. This would give 1/4 f_{ce} cos θ. equal to 2.0 kHz ((see Table 1). As the observed frequency is lower, higher frequencies would arrive first. Increasing frequency of whistler mode signals, notably in chorus and in stimulated emission, is often observed in ground based observations, [*Helliwell*, 1965] as well as space-based [*Hikishima et al.*, 2009; *Verkhoglyadova et al.*, 2009]. *Breneman et al.* [2009] also found that dispersion did not account for the frequency rise, or not all of it. This frequency rise has been the subject of theory and simulation also [*Hikishima et al.*, 2009]. It appears likely that the frequency increase is not due to dispersion. Theory and simulations of frequency increase due to nonlinear effects have been presented by several authors [*Omura et al.*, 2009; *Hikishima et al.*, 2009].

[18] It should be noted that the X antenna system saturates at about 100 mV/m peak, so that a few of the waveform excursions are saturated. The Y and Z antennas, with effective lengths a factor of 10 smaller but different gains, would saturate at about 500 mV/m, but such a large signal has not been observed.

[19] Table 1 shows that several of the episodes are concurrent with large AE index, indicating a substorm in progress or just finished. No AE index is available for the episode in 1998. The two with AE indices below 450 nT are those which are sunward of the Earth in Figure 1. At these positions it would require several hours for electrons of the energy that may possibly excite the waves to drift from an injection point near midnight to the observed position. The highest AE preceding the 2002/10/10 event was 366 nT, reached 12 h earlier, while for 2000/08/15, AE reached 402 nT eight hours before the whistler event, so that both of these are also likely to have been preceded by substorms.

[20] Many whistler events show two frequency bands, as in Figure 2. Since several resonances are possible for electrons of a given velocity, it might be thought that the upper band is a separately generated signal. Instead it is the harmonic of the lower band and such a harmonic is observed in most of the events. Note, however, that the whistler in Figure 3 does not show a harmonic signal. In section 7, some evidence will be presented that the harmonic is due to distortion of the waveform by electron trapping in the electrostatic potential of an oblique whistler. Further, and conclusive evidence in our opinion, is given in a separate paper which combines STEREO and Wind data [*Kellogg et al.*, 2010].

4. Generation of These Whistlers

[21] It would be of considerable interest to see the electron distributions in the region where the whistlers are generated and to see if they are unstable to whistlers like those observed. The event shown in Figure 2 was thought to be a good candidate, as Wind was about 1.2°N in GME coordinates and chorus is generated near the magnetic equator [*Goldstein and Tsurutani*, 1984; *LeDocq et al.*, 1998; *Santolík et al.*, 2005; *Breneman et al.*, 2007, 2009; *Omura et al.*, 2008, 2009; *Agapitov et al.*, 2010]. At the outset there is not much hope of recognizing instability from the plasma data, as the observed whistlers grow and decay in a few milliseconds and it takes 3 s for the Wind plasma experiment, 3DP [*Lin et al.*, 1995], to gather a distribution function. It will be seen that these fears are borne out. Nevertheless we have analyzed the 3DP data for instability at the time of the whistler in Figure 2, and found an instability with several interesting properties, but which may not be generating the whistlers at the place where they are observed.

[22] Figure 4 displays this electron distribution function from the 3DP plasma instrument on Wind. Contours relative to the magnetic field direction (horizontal axis) are shown in

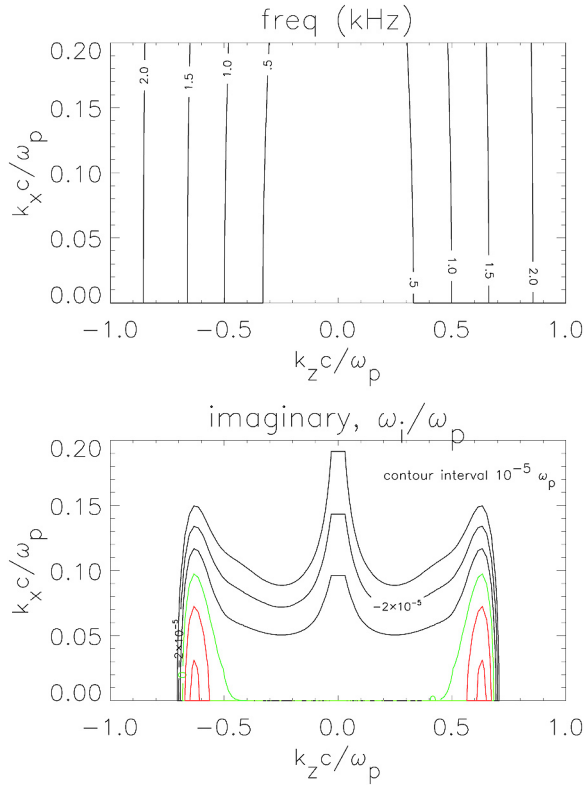

Figure 5. Frequency and growth contours for the bi-Maxwellian distributions of Figure 4.

the upper panel. This distribution is "pancake" shaped at the higher energies. The distribution has been approximated by the sum of two bi-Maxwellians, a low energy distribution which is elongated along field lines, (Tpar = 25 ev, Tperp = 18 ev, fractional density = 0.55), and a high energy pancake distribution (Tpar = 200 eV, Tperp = 300 eV, fractional density = 0.45). In the lower panel are shown parallel and perpendicular cuts through the distribution data (diamonds) and these approximations by the two bi-Maxwellians (solid lines). It can be seen that the approximation is not very good, as electron distributions are known to be not very Maxwellian.

[23] Pancake distributions are unstable, with the free energy coming from the excess of perpendicular energy. *Brice* [1964], referring to *Stix* [1962] gave an elegant picture of these effects. *Kennel and Petschek* [1966] worked out a more complete criterion. For comparison with Kennel and Petschek, the average parallel and perpendicular temperatures are 142 and 208 eV. When these temperatures are put into the Kennel-Petschek criterion for instability [*Kennel and Petschek*, 1966, equation 2.21]:

$$\frac{T_\perp - T_\parallel}{T_\parallel} > \frac{1}{\frac{\Omega_e}{\omega} - 1}$$

the left hand side is 0.46 and the right hand side is smaller, indicating instability, for f = $\omega/2\pi$ less than 1.0 kHz. The maximum of the spectrum of Figure 2 is at 1.25 kHz but the spectrum extends above it. 1.25 kHz corresponds to the limit using the hot temperatures alone. In what follows we will cast doubt on the idea that the whistlers are locally generated, and so we would not expect full consistency with the Kennel-Petschek criterion.

[24] This fit to the distribution has been used with our warm plasma dispersion relation solver "OSCARS" to determine both the real and imaginary parts of the frequency. Figure 5 shows contour plots of the real and imaginary parts of the frequency in the kpar, kperp plane obtained from these solutions. The green line shows zero imaginary part, and the red lines show positive imaginary part. Only three of the negative contours are shown. In order to check, we have also run the popular dispersion solver WHAMP [*Ronnmark*, 1983]. WHAMP is not as accurate as our OSCARS, especially for weak growth, but the growth rate agreed with OSCARS to within 10%.

[25] From Figure 5 it can be seen that the maximum growth rate $\omega_i = 0.226\ 10^{-4}\ \omega_p$, growth time $1/\omega_i = 0.08$ s, occurs for $kc/\omega_p = 0.631$ and $\omega/\omega_p = 0.0156$. $\Omega/\omega_p = 0.055$ so that the resonant velocity for cyclotron resonance $(\Omega - \omega)/k = 0.0624$ c = 1.87 10^4 km s^{-1}, or at an energy of 973 eV. This speed is shown as vertical lines in Figure 4.

[26] However, this instability may not be generating the whistlers that are observed. An analysis of a TDSS event which is close in time to the event of Figure 2 shows that the angle between the wave vector and the magnetic field is 61°. The unstable region of Figure 5 extends only to about 10°. In addition, the observed whistlers grow and decay in a few milliseconds, while this instability is much slower.

[27] Owing to the 3 s accumulation time of 3DP, it is not clear that the observed electron distribution function is an accurate representation of the unstable plasma. We earlier reported that we thought we had found the generation region [*Kellogg et al.*, 2008] but we now think that identification was not correct. It seems most likely that the whistlers were generated elsewhere and propagated to our observations region. However, this idea will be pursued further below.

[28] We have made similar analyses on three other events, chosen because their wave vectors were nearly parallel to B. In one case the distribution appeared to fail to satisfy the Kennel-Petschek criterion for instability locally. Another, which will be shown later as Figure 11, showed a low energy beam. During this event the plasma density is quite low, so that kHz whistlers are too fast to have the expected Landau resonance with this low energy beam at anywhere near the observed frequency and it cannot provide a source for whistlers. The third is the event shown in Figure 3. We do not have accurate wave vector direction for this event, but the absence of a harmonic signal indicates nearly parallel propagation [*Kellogg et al.*, 2010]. This event also occurred at a low magnetic latitude, 2.9°, but at 3.6 R_E was rather closer to the Earth than most events. The instability analysis gave no appreciable instability (growth rate within the errors), though the two bi-Maxwellian approximation did satisfy the Kennel-Petschek criterion for frequency less than 1.8 kHz. Some manipulation of parameters could probably give growth at something like the observed frequency, but the growth would not be as fast as the millisecond variations observed. We therefore have not found a case where the instability analysis agrees both in frequency and wave vector direction with the observations, and therefore no evidence that any of the observed whistlers were generated where we observed them.

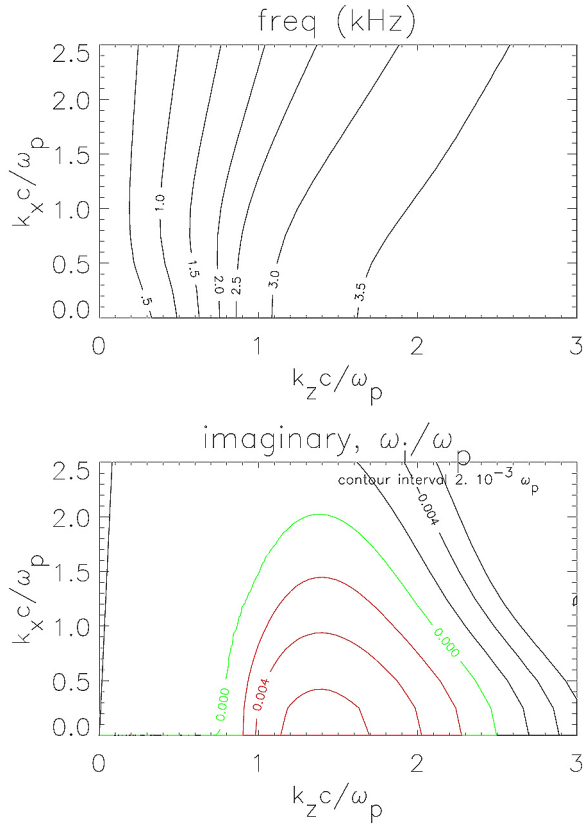

Figure 6. Frequency and growth contours for an extremely anisotropic distribution.

[29] Because the time required for 3DP to collect an electron distribution, 3 s, is so long compared to the duration of these large amplitude whistlers, we speculate on possible instabilities that are consistent with the observations. It seems reasonable that the rapidly growing whistler might feed on the perpendicular electron velocity, and that therefore the observed distribution function has been strongly isotropized by pitch angle scattering [*Horne et al.*, 2003]. We are led, therefore, to consider a (short-lived) more strongly anisotropic distribution. If the parallel temperature of the hot component is taken to be the same (30 eV) as that of the cold component, and the rest of the hot energy is put into the perpendicular temperature, the perpendicular temperature is then 390 eV, an extreme case. Figure 6 shows the growth and frequency contours for this case. Both the growth rate and the pitch angle for growth are strongly increased. Maximum growth occurs for a frequency of 3.5 kHz, and the growth time, 1.5 m s^{-1}, is very much shorter than found in Figure 5. Growth continues out to wave vector-B angles of 60°. The frequency, of course, does not correspond to the observed frequency. Further, even though the extreme case allows growth near the observed pitch angle, nevertheless the fastest growth is for parallel whistlers. However, it seems that this idea, that the observed distribution functions are only the remnants of the generating distribution, might be further pursued. At present, it seems most likely that the whistlers are generated elsewhere, perhaps even by a different process such as by a beam, and continue to be amplified as they pass through the observation region.

[30] As mentioned above, the telemetry devoted to the slow TDS, TDSS, was less than that devoted to TDSF. Hence three useable components of magnetic field are available for only 11 events of the 5 large amplitude episodes. From these, the direction of the wave vector, k, with respect to the magnetic field could be determined. Since the whistlers consist of a mixture of waves, none of the eigenvalues of the variance matrix are actually zero. As is usual practice, the direction of k has been taken to be the direction of the eigenvector corresponding to the smallest eigenvalue. A histogram of these directions is shown as Figure 7. It will be seen that the directions are principally at small angles, an effect which would be even more prominent if the histogram had been normalized to available solid angle, which was not done. The largest angle found was 48°. Although the directions are clustered around the magnetic field direction, they still cover a wider range than would be expected from the contour plots of growth of Figures 5 and 6, which are strongly indicative of small angles. Again it may be that the wave vectors have been changed to larger angles during propagation from their source to the observation point, or it may be that the distribution function is changing rapidly.

[31] *Cattell et al.* [2008] found even more oblique wave vectors for their observations. This question of propagation versus local generation remains unanswered.

5. Acceleration of Electrons

[32] Fields of 100 mV/m present evident possibilities for acceleration of electrons. A number of authors [*Summers et al.*, 1998; *Horne and Thorne*, 1998; *Horne et al.*, 2005; *Bortnik et al.*, 2008] have considered the cyclotron resonance, in which the electrons can remain in the associated electric field for many revolutions and gain considerable energy. As the rate of energy gain is eE.v, where *v* is the electron velocity, the process is more effective on initially energetic particles than on thermal particles. A 250 eV electron in a 100 mV/m whistler, and with the field parameters of 2002/10/10 will gain 60 eV per revolution, and so will not be a 250 eV electron for long. *Roth et al.* [1999] as

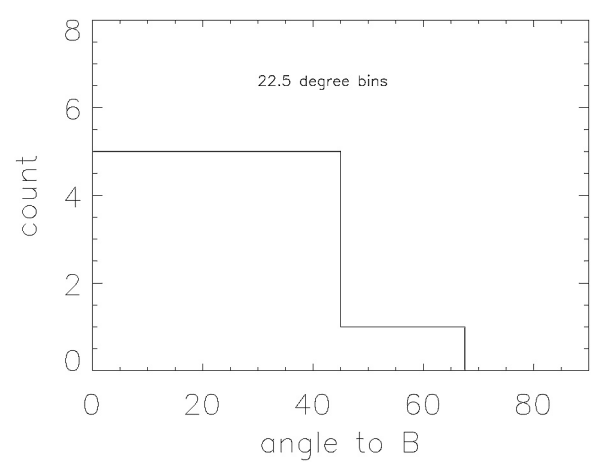

Figure 7. Histogram of angle between the wave vector **k** and the magnetic field B_0.

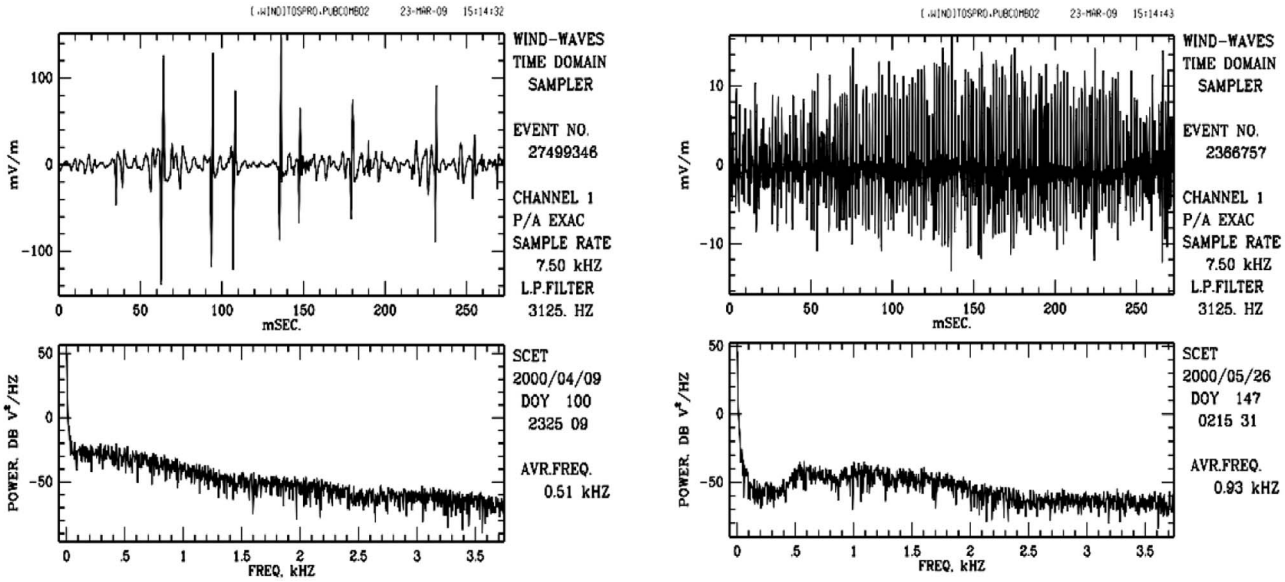

Figure 8. Time series of two episodes of electron holes. These represent some extremes of observed occurrence rates.

well as some authors quoted above, have combined this mechanism with the divergence of B in the Earth's dipole field to reflect electrons and to accelerate electrons to MeV ranges. Recently, *Omura et al.* [2007] have extended this work, showing that electrons of hundreds of keV can be accelerated to the MeV range. *Cattell et al.* [2008] also simulated the interaction of whistlers like those observed here and also showed that electrons could be accelerated by these whistlers to MeV energies in a very short time (fractions of a second). Further studies of this mechanism are in progress by various groups, but further consideration here is beyond the scope of this work.

6. Electron Holes

[33] Adjacent in time to the regions where whistlers were observed Wind-Waves observed large numbers of what are believed to be electron holes. The large whistlers were often "sandwiched" between hole episodes. This phenomenon as observed by frequency domain instruments was first

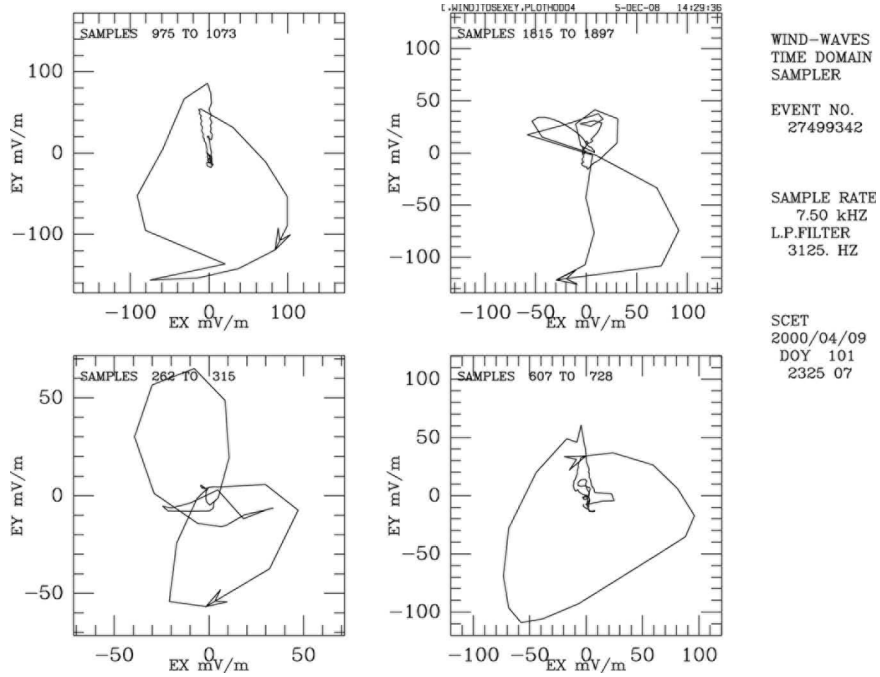

Figure 9. Hodograms of some of the stronger holes shown in Figure 8.

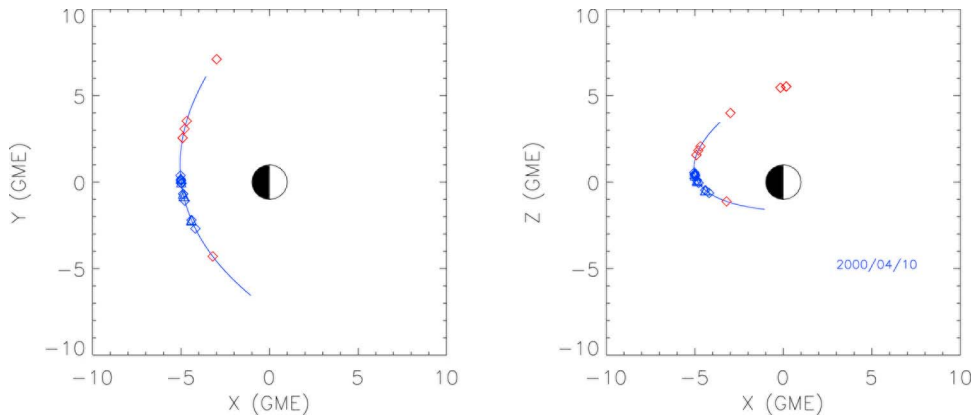

Figure 10. Locations of electron holes (red) and whistlers (blue) for the episodes of Figures 2–6 and Figure 7.

described as Broadband Electrostatic Noise (BEN) [*Gurnett and Frank*, 1977], and was later recognized as a series of "spikes" using the time domain instrument on GEOTAIL [*Matsumoto et al.*, 1994]. Similar observations have been reported by a number of authors [e.g., *Carlson et al.*, 1998; *Andersson et al.*, 2009]. Studies which include a more complete discussion of the physics of such holes, including identification and electron BGK modes, have been made by *Ergun et al.* [1998a, 1998b]. Observation of electron holes in various regions of the magnetosphere have been discussed by *Cattell et al.* [1999, 2001a, 2001b, 2003]. A recent study has been made with Cluster instruments [*Pickett et al.*, 2004]. The observations presented here are of considerably higher amplitude than those observed by Pickett *et al.* The TDS instrument picks out the largest signal among a series of events, the TDS saturation level is higher than that of the Cluster instrument, so that it is not clear that there is any inconsistency. Two examples, to demonstrate the extremes of occurrence rate and of amplitude, are shown in Figure 8. It will be noted that these are quite similar to the events reported by *Ergun et al.* [1998a, 1998b]. One has the impression from the right panel of Figure 8 that the repetition rate of the holes is regular, and that the holes are spaced by roughly 2 msec. Confirming this, the spectrum shows a peak at the corresponding 500 Hz. This frequency is close to the lower hybrid frequency, as was earlier found by *Ergun et al.* [1998b]. In Figure 9 are shown two dimensional hodograms of four of the strongest signals of Figure 8 showing the characteristic signature of traversal of holes by a spacecraft, bipolar in one direction and monopolar in the other.

[34] Definitive identification of these solitary waves as electron, and not ion, holes, requires knowledge of the direction in which the hole is crossing the spacecraft and physical scale sizes and potential amplitudes require knowledge of the structure speed. In all respects the solitary waves observed in these Wind passes are essentially the same as those reported by *Ergun et al.* [1998a, 1998b] and *Cattell et al.* [1999], who did identify the solitary waves as electron holes using measurements of the structure velocity.

[35] In Figure 10 are shown the locations, on one particular orbit, where these holes were observed by Wind-Waves together with the large whistlers described above. The red symbols indicate holes and the blue symbols indicate whistlers. It is fairly certain that the region of electron holes extends both earlier and later than shown, but the sampling rate before and after the intervals shown had been changed to a rate too small to clearly resolve the holes. As these are typical it appears that the large whistler episodes are often

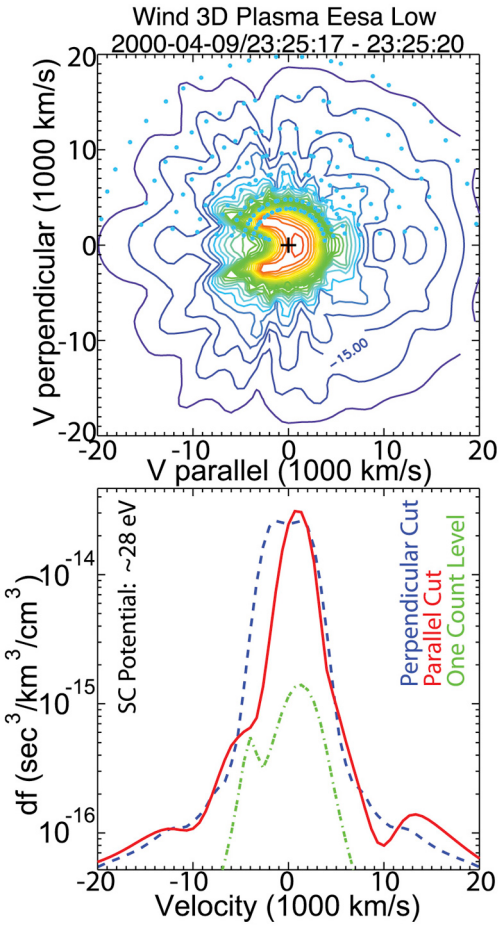

Figure 11. An electron distribution function near the period of part of Figure 9.

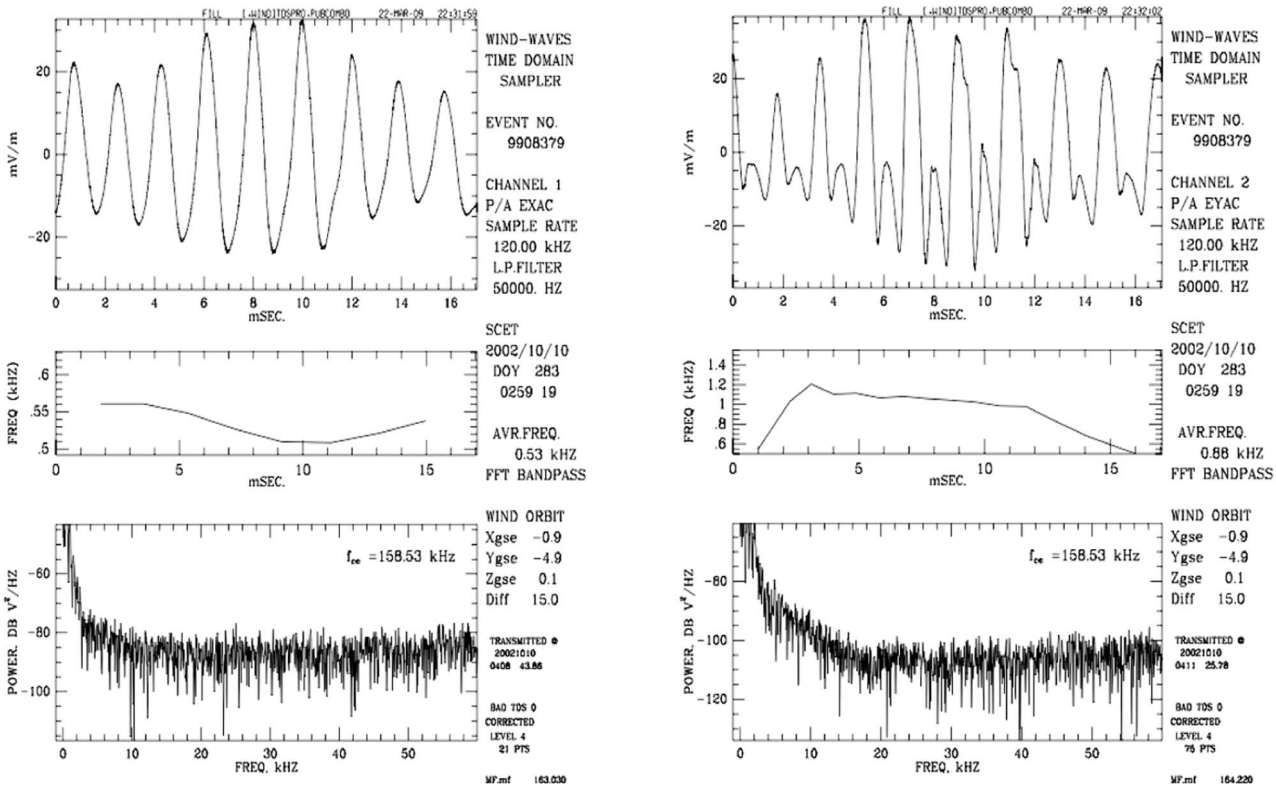

Figure 12. Waveforms showing a distortion due to trapped electrons.

preceded and/or followed by episodes of electron holes. This association may occur because the free energy sources for both phenomena are associated with substorms.

[36] Electron holes are often associated with current, or Buneman, instabilities. Even very early simulations showed the process of overturning and trapping in such an instability. Figure 11 shows an electron distribution function during this episode of electron holes corresponding to the time of the left hand panel of Figure 8 and of Figure 9. It shows a directed electron beam at about 13000 km s^{-1} (46 eV), as well as a loss cone, corresponding to expectations for electron hole formation.

7. Trapping

[37] During the episode of 2002/10/10, events were captured which have some other very interesting characteristics. Some example waveforms are shown as Figure 12. During these events, the sample rate of the fast TDS, TDSF, was set to its fastest rate, 120 ksamples s^{-1}. This was, unfortunately, the only episode where the fastest rate was in use during these five Wind episodes. It will be seen that there is a strange distortion of the negative peaks of the waveforms. This distortion is much less severe in the X antenna. In another paper [*Kellogg et al.*, 2010] it is shown that the distortion is due to electrons trapped at a certain phase of the whistler. These electrons then form a sheet which moves with the whistler, and generate a linearly polarized electrostatic field which is aligned with the wave vector. The distortion signal then must be more closely aligned with the Y antenna.

[38] These effects are also observed in the STEREO/Waves events. Figure 13 shows a short section of data during the episode reported by *Cattell et al.* [2008]. The upper curve shows that whole event, and the lower panels show the signals in a coordinate system aligned along **B**. It will be seen that again the signature of electron trapping is stronger on one of the antennas. It is presumed that this signature is from an electron bunch trapped at a certain wave phase. The electric field of such trapped electrons would be expected to be parallel to the wave vector, and so it can be used to determine the direction of the wave vector from electric field data.

[39] Two kinds of electron trapping by whistlers have been discussed in the literature. Electron trapping was discussed by *Matsumoto and Omura* [1981] and by *Omura and Matsumoto* [1982], but was discussed earlier in the context of stimulated emissions by *Nunn* [1971]. One kind is trapping in a certain phase at the cyclotron resonance, where the electrons see a rotating electric field which can accelerate or decelerate them. This trapping has received the most attention [e.g., *Matsumoto and Omura*, 1981; *Bortnik et al.*, 2008] as it may be possible to impart considerable energy to electrons that can make many revolutions before leaving the trap.

[40] Here we are seeing a different trapping. [e.g., *Kumagai et al.*, 1980]. These electrons see a DC field. We show in another paper [*Kellogg et al.*, 2010] that the distortion is trapping of electrons at the maxima of the electric potential associated with the longitudinal electric component of an oblique whistler. That the distortion is due to an electric field resulting from charge and not from induction is

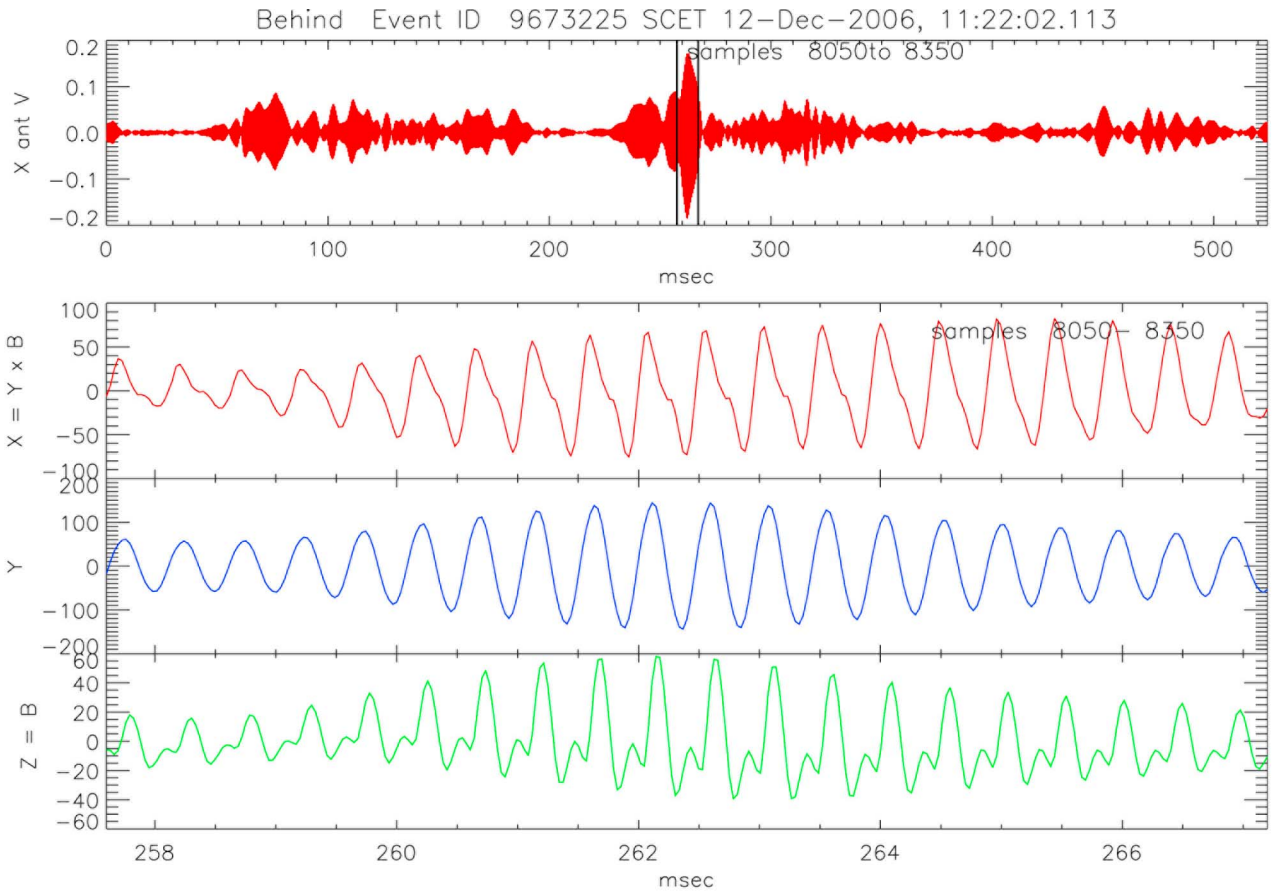

Figure 13. Waveforms observed by STEREO-S/WAVES showing the same electron-trapping distortion.

shown in Figure 14 which displays a whistler of the same episode captured by the TDSS, which at this time was connected to one electric antenna, and to the three axes of the search coils. It will be seen that the harmonic of the main signal is present on the electric antenna, but absent on the search coil, so that the distorting field is electrostatic. We interpret the harmonic, here as well as in Figure 2 (and its absence in Figure 3) as due to electron trapping (or a lack of it). We note that a majority of the Wind whistlers show this distortion, although the sampling rate was often not sufficient to resolve the trapping feature clearly, and so such trapping is quite common. Since they are trapped at a potential energy minimum, only limited acceleration is possible while they remain trapped. Whether they gain or lose energy in being trapped will depend on the relative number of faster and slower electrons in the original distributions, as it does for Langmuir wave generation, for example.

[41] In these observations with Wind-Waves, there are two pieces of evidence in favor of our interpretation that the distorting signal comes from charge sheets trapped at a certain phase of the longitudinal part of an oblique whistler, one that the distortion is electrostatic (Figure 14) and so involves some charge which moves with the whistler, and two that nearly parallel propagating whistlers (Figure 3) do not show the signature which we interpret as trapping.

[42] Further investigation of this trapping process has been done with the STEREO data, which measures electric fields in three dimensions [*Kellogg et al.*, 2010].

8. Summary and Conclusions

[43] We have described the results of a statistical survey of large amplitude (hundreds of mV/m) waveforms in the magnetosphere inside ~10 Re. Two types of waves were found to frequently occur: (1) nearly monochromatic whistler waves primarily at radial distances inside ~6 Re and near or within the plasmasphere and plasmapause, and (2) solitary waves at larger radial distances on plasma sheet and auroral field lines. The Wind-Waves observations of the whistler waves have provided two new results to the previous studies of large amplitude whistlers by *Cattell et al.* [2008] and *Cully et al.* [2008]. Out of 17 perigees, large amplitude whistlers (~100 mV/m in electric field) were seen in five, showing that these whistlers are fairly common. The whistlers are very bursty, with large amplitudes only lasting msec. The harmonic distortions of the electric field waveforms have been shown to be consistent with trapping of electrons in the whistlers [*Kellogg et al.*, 2010]. In addition, because Wind-Waves obtained 3D search coil measurements for some events, the wave vectors could be directly determined for large amplitude whistlers.

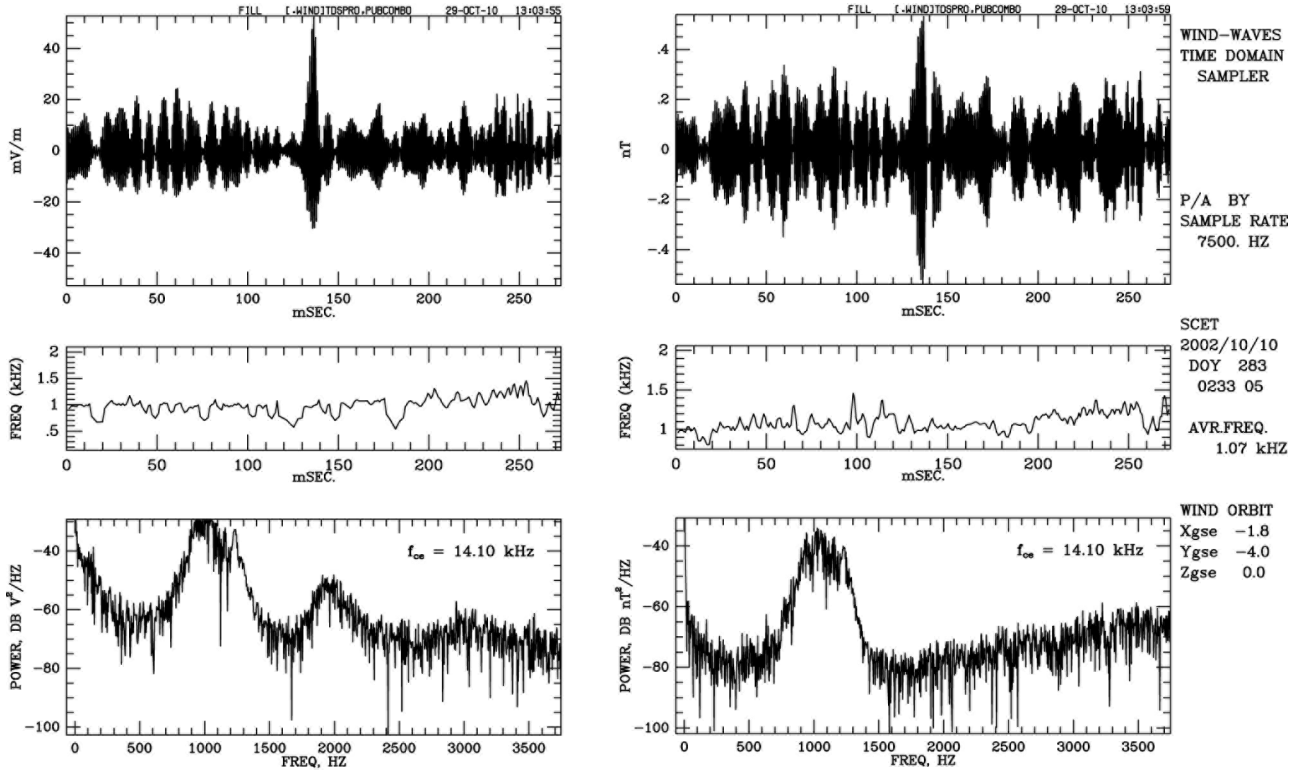

Figure 14. Electric and magnetic spectra showing that the harmonic distortion is purely electric.

The observed waves propagated at angles varying from parallel to the magnetic field to very oblique (48°).

[44] Simultaneously observed electron distributions were used as inputs to a warm dispersion solver to examine instability mechanisms. In at least one case, the magnetospheric plasma was shown to be unstable to a Kennel-Petschek type instability locally, but the wave vector angle and frequency suggested that the observed whistler had come from elsewhere, or that the electron distribution function had significantly altered during 3 s, or both. As the instability found here tends to create whistlers with a smaller angle to B than the observed angles up to 48°, it seems that this angle must generally have increased during propagation from a more distant source.

[45] Our observations are consistent with the widely accepted picture that electrons are injected from the plasma sheet of the magnetotail during substorms, and that they diffuse while conserving magnetic moment, at least partially, and so those diffusing inward form an energized pancake distribution [*Kellogg*, 1959].

[46] Evidence of significant trapping of electrons in these whistlers is presented. Most of the waveforms show a large distortion shown by the presence of harmonics in the spectrum. For one Wind episode and all of the STEREO episodes, the sample rate was large enough to display the nature of this distortion clearly, and it is consistent with trapping of electrons at a fixed phase of the whistler. These trapped electrons occur only for obliquely propagating whistlers, and are elsewhere shown to be due to trapping in the electrostatic part of an oblique whistler [*Kellogg et al.*, 2010]. Phase trapping, in which the electrons are uniformly distributed in space but are non-gyrotropic would not be consistent with the observations.

[47] These large whistlers are considered to be capable of accelerating electrons to considerable energies, as discussed by *Cattell et al.* [2008] and others, and perhaps account for the most energetic electrons of the radiation belts. The interaction of whistlers with weakly relativistic electrons has also been recently invoked as an acceleration mechanism by *Omura et al.* [2007]. That process, which is nonlocal, is, however, different from simple trapping.

[48] In many cases, the episodes of intense whistlers are preceded and/or followed by episodes of intense electrostatic solitary waves, interpreted as electron holes. The holes are found before and after the whistlers, and at times have high repetition rates. Examples are presented and one example is shown to be the result of electron beams, but the relation of these holes to the physics of the magnetosphere is not pursued further.

[49] **Acknowledgments.** This work was supported by the National Aeronautics and Space Administration under grants NNX07AF23G (STEREO), NNX11AB46G, NESSF grant NNX07AU72H, and NNX07AM97G and NNX08AT81G (Wind). L. B. W was partially supported by a Dr. L. Burlaga/Arctowski Medal Fellowship. We thank R. Lepping, GSFC, and C. T. Russell, UCLA, and CDAWeb for the magnetic field and density data, and for the electron distribution and ion density data we thank R. Lin, UCBerkeley. We also thank Robert L. Lysak and a reviewer for valuable discussions of the instability.

[50] Philippa Browning thanks the reviewers for their assistance in evaluating paper 2010JA015919.

References

Agapitov, O., V. Krasnoselskikh, Y. Zaliznyak, V. Angelopoulos, O. Le Contel, and G. Rolland (2010), Chorus source region localization in the Earth's outer magnetosphere using THEMIS measurements, *Ann. Geophys.*, *28*, 1377–1386, doi:10.5194/angeo-28-1377-2010.

Andersson, L., et al. (2009), New features of electron phase space holes observed by the THEMIS mission, *Phys. Rev. Lett.*, *102*(22), doi:10.1103/PhysRevLett.102.225004.

Bortnik, J., R. M. Thorne, and U. S. Inan (2008), Nonlinear interaction of energetic electrons with large amplitude chorus, *Geophys. Res. Lett.*, *35*, L21102, doi:10.1029/2008GL035500.

Bougeret, J.-L., et al. (1995), WAVES: The radio and plasma wave investigation on the Wind spacecraft, *Space Sci. Rev.*, *71*, 231–263, doi:10.1007/BF00751331.

Bougeret, J. L., et al. (2008), S/WAVES: The radio and plasma wave investigation on the STEREO mission, *Space Sci. Rev.*, *136*(1–4), 487–528, doi:10.1007/s11214-007-9298-8.

Breneman, A., C. A. Kletzing, J. Chum, O. Santolík, D. Gurnett, and J. Pickett (2007), Multispacecraft observations of chorus dispersion and source location, *J. Geophys. Res.*, *112*, A05221, doi:10.1029/2006JA012058.

Breneman, A. W., C. A. Kletzing, J. Pickett, J. Chum, and O. Santolík (2009), Statistics of multispacecraft observations of chorus dispersion and source location, *J. Geophys. Res.*, *114*, A06202, doi:10.1029/2008JA013549.

Brice, N. (1964), Fundamentals of very low frequency emission generation mechanisms, *J. Geophys. Res.*, *69*(21), 4515–4522, doi:10.1029/JZ069i021p04515.

Carlson, C. W., et al. (1998), FAST observations in the downward auroral current region: Energetic upgoing electron beams, parallel potential drops, and ion heating, *Geophys. Res. Lett.*, *25*(12), 2017–2020, doi:10.1029/98GL00851.

Cattell, C. A., et al. (1999), Comparisons of Polar satellite observations of solitary wave velocities in the plasma sheet boundary and the high altitude cusp to those in the auroral zone, *Geophys. Res. Lett.*, *26*(3), 425–438, doi:10.1029/1998GL900304.

Cattell, C., et al. (2001a), Comparisons of solitary waves and wave packets observed at plasma sheet boundary to results from the auroral zone, *Phys. Chem. Earth*, *26*, 97–106.

Cattell, C., J. Crumley, J. Dombeck, R. Lysak, C. Kletzing, W. K. Peterson, and H. Collin (2001b), Polar observations of solitary waves at high and low altitudes and comparison to theory, *Adv. Space Res.*, *28*, 1631–1641, doi:10.1016/S0273-1177(01)00478-1.

Cattell, C., C. Neiman, J. Dombeck, J. Crumley, J. Wygant, C. A. Kletzing, W. K. Peterson, F. S. Mozer, and M. André (2003), Large amplitude solitary waves in and near the Earth's magnetosphere, magnetopause and bow shock: Polar and Cluster observations, *Nonlinear Process. Geophys.*, *10*, 13–26, doi:10.5194/npg-10-13-2003.

Cattell, C., et al. (2008), Discovery of very large amplitude whistler-mode waves in Earth's radiation belts, *Geophys. Res. Lett.*, *35*, L01105, doi:10.1029/2007GL032009.

Cully, C. M., J. W. Bonnell, and R. E. Ergun (2008), THEMIS observations of long-lived regions of large-amplitude whistler waves in the inner magnetosphere, *Geophys. Res. Lett.*, *35*(17), L17S16, doi:10.1029/2008GL033643.

Ergun, R. E., et al. (1998a), FAST satellite observations of large-amplitude solitary structures, *Geophys. Res. Lett.*, *25*(12), 2041–2044, doi:10.1029/98GL00636.

Ergun, R. E., C. W. Carlson, J. P. McFadden, F. S. Mozer, L. Muschietti, I. Roth, and R. J. Strangeway (1998b), Debye-scale plasma structures associated with magnetic-field-aligned electric fields, *Phys. Rev. Lett.*, *81*(4), 826–829, doi:10.1103/PhysRevLett.81.826.

Goldstein, B. E., and B. T. Tsurutani (1984), Wave normal directions of chorus near the equatorial source region, *J. Geophys. Res.*, *89*(A5), 2789–2810, doi:10.1029/JA089iA05p02789.

Gurnett, D. A., and L. A. Frank (1977), A region of intense plasma wave turbulence on auroral field lines, *J. Geophys. Res.*, *82*(7), 1031–1050, doi:10.1029/JA082i007p01031.

Helliwell, R. A. (1965), *Whistlers and Related Ionospheric Phenomena*, Stanford Univ. Press, Stanford, Calif.

Hikishima, M., S. Yagitani, Y. Omura, and I. Nagano (2009), Full particle simulation of whistler-mode rising chorus emissions in the magnetosphere, *J. Geophys. Res.*, *114*(A1), A01203, doi:10.1029/2008JA013625.

Horne, R. B., and R. M. Thorne (1998), Potential waves for relativistic electron scattering and stochastic acceleration during magnetic storms, *Geophys. Res. Lett.*, *25*(15), 3011–3014, doi:10.1029/98GL01002.

Horne, R. B., S. A. Glauert, and R. M. Thorne (2003), Resonant diffusion of radiation belt electrons by whistler-mode chorus, *Geophys. Res. Lett.*, *30*(9), 1493, doi:10.1029/2003GL016963.

Horne, R. B., et al. (2005), Wave acceleration of electrons in the Van Allen radiation belts, *Nature*, *437*, 227–230, doi:10.1038/nature03939.

Kellogg, P. J. (1959), Van Allen radiation of solar origin, *Nature*, *183*, 1295, doi:10.1038/1831295a0.

Kellogg, P. J., C. A. Cattell, S. J. Monson, and K. Goetz (2008), Large amplitude whistlers observed by wind-waves, *Eos Trans. AGU*, *89*(53), Fall Meet. Suppl., Abstract SM42A–06.

Kellogg, P. J., C. A. Cattell, K. Goetz, S. J. Monson, and L. B. Wilson III (2010), Electron trapping and charge transport by large amplitude whistlers, *Geophys. Res. Lett.*, *37*, L20106, doi:10.1029/2010GL044845.

Kennel, C. F., and H. E. Petschek (1966), Limits on stably trapped particle fluxes, *J. Geophys. Res.*, *71*, 1–18.

Kumagai, H., K. Hashimoto, I. Kimura, and H. Matsumoto (1980), Computer simulation of a Cerenkov Interaction between obliquely propagating whistler mode waves and an electron beam, *Phys. Fluids*, *23*, 184–201, doi:10.1063/1.862837.

LeDocq, M. J., D. A. Gurnett, and G. B. Hospodarsky (1998), Chorus source locations from VLF Poynting flux measurements with the Polar spacecraft, *Geophys. Res. Lett.*, *25*(21), 4063–4066, doi:10.1029/1998GL900071.

Lin, R. P., et al. (1995), A three-dimensional plasma and energetic particle investigation for the WIND spacecraft, *Space Sci. Rev.*, *71*(1–4), 125–153, doi:10.1007/BF00751328.

Matsumoto, H., and Y. Omura (1981), Cluster and channel effect phase bunchings by whistler waves in the nonuniform geomagnetic field, *J. Geophys. Res.*, *86*(A2), 779–791, doi:10.1029/JA086iA02p00779.

Matsumoto, H., H. Kojima, T. Miyatake, Y. Omura, M. Okada, I. Nagano, and M. Tsutsui (1994), Electrostatic solitary waves (ESW) in the magnetotail: BEN wave forms observed by GEOTAIL, *Geophys. Res. Lett.*, *21*(25), 2915–2918, doi:10.1029/94GL01284.

Millan, R. M., and R. M. Thorne (2007), Review of radiation belt relativistic electron losses, *J. Atmos. Sol. Terr. Phys.*, *69*(3), 362–377, doi:10.1016/j.jastp.2006.06.019.

Nunn, D. (1971), A theory of VLF emissions, *Planet. Space Sci.*, *19*, 1141–1167, doi:10.1016/0032-0633(71)90110-3.

Omura, Y., and H. Matsumoto (1982), Computer simulations of basic processes of coherent whistler wave-particle interactions in the magnetosphere, *J. Geophys. Res.*, *87*(A6), 4435–4444, doi:10.1029/JA087iA06p04435.

Omura, Y., N. Furuya, and D. Summers (2007), Relativistic turning acceleration of resonant electrons by coherent whistler-mode waves in a dipole magnetic field, *J. Geophys. Res.*, *112*(A6), A06236, doi:10.1029/2006JA012243.

Omura, Y., Y. Katoh, and D. Summers (2008), Theory and simulation of the generation of whistler-mode chorus, *J. Geophys. Res.*, *113*, A04223, doi:10.1029/2007JA012622.

Omura, Y., M. Hikishima, Y. Katoh, D. Summers, and S. Yagitani (2009), Nonlinear mechanisms of lower-band and upper-band VLF chorus emissions in the magnetosphere, *J. Geophys. Res.*, *114*, A07217, doi:10.1029/2009JA014206.

Pickett, J. S., et al. (2004), Solitary waves observed in the auroral zone: The Cluster multi-spacecraft perspective, *Nonlinear Process. Geophys.*, *11*, 183–196, doi:10.5194/npg-11-183-2004.

Ronnmark, K. (1983), Computation of the dielectric tensor of a Maxwellian plasma, *Plasma Phys.*, *25*(6), 699–701, doi:10.1088/0032-1028/25/6/007.

Roth, I., M. Temerin, and M. K. Hudson (1999), Resonant Enhancement of Relativistic Electron Fluxes During Geomagnetically Active Periods, *Ann. Geophys.*, *17*, 631, doi:10.1007/s00585-999-0631-2.

Santolík, O., D. A. Gurnett, J. S. Pickett, M. Parrot, and N. Cornilleau-Wehrlin (2003), Spatio-temporal structure of storm-time chorus, *J. Geophys. Res.*, *108*(A7), 1278, doi:10.1029/2002JA009791.

Santolík, O., D. A. Gurnett, J. S. Pickett, M. Parrot, and N. Cornilleau-Wehrlin (2005), Central position of the source region of storm-time chorus, *Planet. Space Sci.*, *53*(1–3), 299–305, doi:10.1016/j.pss.2004.09.056.

Stix, T. H. (1962), *The Theory of Plasma Waves*, McGraw-Hill Book Company, New York.

Summers, D., R. M. Thorne, and F. Xiao (1998), Relativistic theory of wave-particle resonant diffusion with application to electron acceleration in the magnetosphere, *J. Geophys. Res.*, *103*(A9), 20,487–20,500, doi:10.1029/98JA01740.

Verkhoglyadova, O. P., B. T. Tsurutani, Y. Omura, and S. Yagitani (2009), Properties of dayside nonlinear rising tone chorus emissions at large *L* observed by GEOTAIL, *Earth Planets Space*, *61*(5), 625–628.

Wilson, L. B., III, C. A. Cattell, P. J. Kellogg, J. R. Wygant, K. Goetz, A. Breneman, and K. Kersten (2011), The properties of large amplitude whistler mode waves in the magnetosphere: Propagation and relationship with geomagnetic activity, *Geophys. Res. Lett.*, doi:10.1029/2011GL048671, in press.

C. A. Cattell, K. Goetz, P. J. Kellogg, and S. J. Monson, School of Physics and Astronomy, University of Minnesota, 116 Church St. SE, Minneapolis, MN 55455, USA. (pauljkellogg@gmail.com)

L. B. Wilson III, Heliophysics Division, NASA/GSFC, Code 672, Rm. 143A, Bldg. 21, Greenbelt, MD 20707, USA.